Fluids and Barriers of the CNS

RESEARCH

Open Access

Navigating the blood–brain barrier to blood–brain tumor barrier transition: microvascular P-glycoprotein and CD146 potentially contribute to glioma grading

Alessia Mora[1†], Francesco Girolamo[1†], Andrea Marzullo[2], Tiziana Annese[3], Michela De Giorgis[1], Francesco Signorelli[4], Raffaella Messina[4], Giuseppe Ingravallo[2], Daniela Virgintino[1], Mariella Errede[1†] and Antonio d'Amati[1,5*†]

Abstract

Background Adult-type diffuse gliomas are highly vascular malignant tumors of the central nervous system (CNS), classified according to the 2021 WHO CNS criteria. Their neovasculature arises through both angiogenesis and vascular co-option, generating heterogeneous microvascular patterns, often associated with microvascular proliferations (MVPs). The transition from an intact blood–brain barrier (BBB) to a dysfunctional blood–brain tumor barrier (BBTB) involves progressive disruption of the neurovascular unit (NVU), yet the phenotypic identity of tumor-associated endothelial cells (ECs) remains poorly characterized.

Methods We investigated the endothelial phenotype in 22 adult-type diffuse gliomas (glioblastoma, astrocytoma grade 4 and 3, oligodendroglioma grade 3 and 2) by immunohistochemical analysis of two EC markers: P-glycoprotein (P-gp), a transporter associated with mature BBB phenotype, and CD146, an adhesion molecule linked to immature, mesenchymal-like ECs. Expression was assessed in the vascular endothelium, perivascular, and extravascular compartments using both qualitative evaluation and morphometric quantification on digital slides.

Results Our findings revealed heterogeneous expression patterns of P-gp and CD146 among glioma subtypes. P-gp expression decreased progressively from oligodendrogliomas to glioblastomas, in line with increasing vascular dedifferentiation. Conversely, CD146 expression was higher in high-grade tumors, particularly in proliferating vessels and perivascular regions. These opposing trends reflected a gradual phenotypic shift from BBB-like to BBTB-like microvasculature, correlating with tumor histotype and grade.

†Alessia Mora and Francesco Girolamo contributed equally to this work.

†Mariella Errede and Antonio d'Amati contributed equally to the work and share last authorship.

*Correspondence:
Antonio d'Amati
damatiantonio@yahoo.it

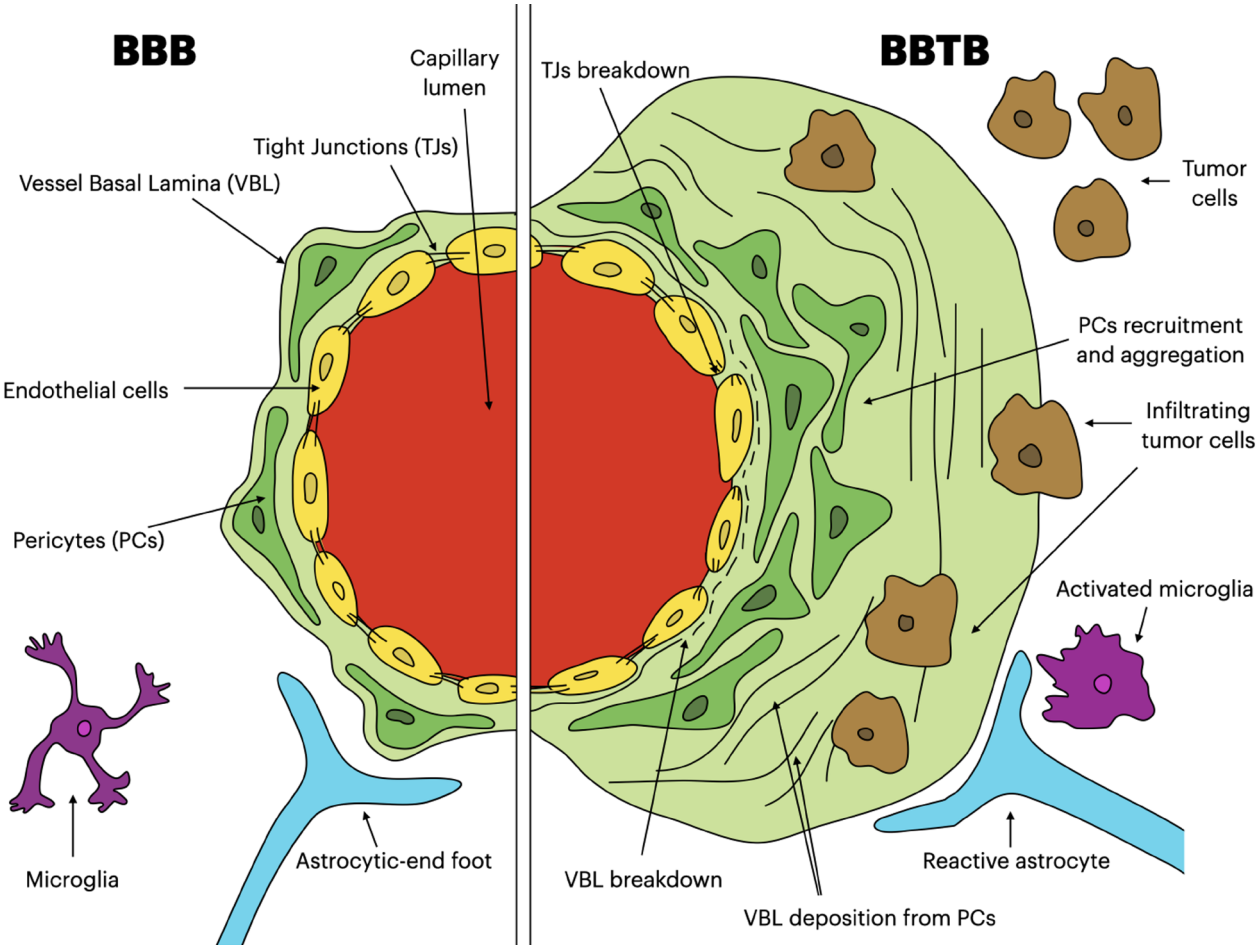
Full list of author information is available at the end of the article

© The Author(s) 2025. **Open Access** This article is licensed under a Creative Commons Attribution-NonCommercial-NoDerivatives 4.0 International License, which permits any non-commercial use, sharing, distribution and reproduction in any medium or format, as long as you give appropriate credit to the original author(s) and the source, provide a link to the Creative Commons licence, and indicate if you modified the licensed material. You do not have permission under this licence to share adapted material derived from this article or parts of it. The images or other third party material in this article are included in the article's Creative Commons licence, unless indicated otherwise in a credit line to the material. If material is not included in the article's Creative Commons licence and your intended use is not permitted by statutory regulation or exceeds the permitted use, you will need to obtain permission directly from the copyright holder. To view a copy of this licence, visit http://creativecommons.org/licenses/by-nc-nd/4.0/.

Conclusion P-gp and CD146 represent complementary markers of endothelial identity in gliomas and may serve as histopathological indicators of BBB integrity and tumor vascular remodeling. Their combined evaluation offers a novel insight into the BBB–BBTB transition and may support microvascular phenotyping as an adjunct criterion for glioma grading.

Keywords Adult-type diffuse gliomas, Microvessel patterns, Blood–brain barrier, Blood–brain-tumor barrier, P-gp, CD146

Graphical abstract



Background

Adult-type diffuse gliomas are a group of malignant central nervous system (CNS) tumors that primarily affect the cerebral hemispheres in adults and are characterized by diffuse infiltration, high vascularization, and variable prognosis. According to the 2021 WHO Classification of Tumors of the Central Nervous System, they are divided into three molecularly and histologically distinct types: Astrocytoma, IDH-mutant, which includes WHO grades 2, 3, and 4; Oligodendroglioma, IDH-mutant, 1p/19q co-deleted, classified as WHO grade 2 or 3; Glioblastoma, IDH-wildtype, which is intrinsically a WHO grade 4 tumor [1–3].

Despite advances in integrated diagnostics and multimodal therapies, including maximal safe resection, radiotherapy, and chemotherapy, the prognosis of diffuse gliomas remains poor, especially for glioblastoma. Overall survival (OS) varies significantly across tumor types and grades, with glioblastoma showing a median OS of 15–18 months, astrocytoma grade 4 approximately 3 years, grade 3 up to 5–10 years, oligodendroglioma grade 3 around 14 years, and grade 2 over 17 years [4, 5].

In addition to molecular features, classical histopathological markers—such as microvascular proliferation (MVP) and necrosis—remain pivotal for tumor grading. The vascular architecture of gliomas can be highly complex and includes distinctive patterns such as

microvascular sprouting, vascular clusters, garlands, and glomeruloid vessels, which are more frequently associated with high-grade gliomas such as glioblastoma and high-grade astrocytoma and oligodendroglioma (Supplementary Fig. 1) [6].

Glioma vascularization results from both the recruitment of pre-existing vessels (vascular co-option) and newly formed vessels via angiogenesis and vasculogenesis. These processes are tightly connected to the functional integrity of the blood–brain barrier (BBB), which is often compromised in high-grade gliomas [7]. The BBB is primarily formed by endothelial cells (ECs) connected by tight junctions, supported by pericytes and basal lamina, and surrounded by astrocyte end-feet and microglia cells, all components of the neurovascular unit (NVU). The involvement of the BBB and of the cellular and molecular components of the NVU in the tumoral, angioformative events leads to a large spectrum of BBB-microvessel dysfunctions denoted as blood–brain tumor barrier (BBTB). The BBTB identifies a microvascular pathological state characterized by altered permeability, perivascular edema, and heterogeneous drug delivery, ultimately contributing to therapy resistance and tumor progression [8–13].

Recent literature has increasingly emphasized the diagnostic and prognostic relevance of vascular alterations in gliomas. Digital pathology and morphometric approaches have been employed to quantify microvascular patterns and support histological grading. At the same time, studies focusing on BBB/NVU dysfunction have underscored the dynamic nature of the BBB–BBTB transition, highlighting the loss of tight junctions, endothelial plasticity, and barrier heterogeneity [14–18]. Despite the crucial role of vascular abnormalities in tumor biology and definitive correlation with poor therapeutic response and prognosis are well established [19–25], little is known about the phenotypic profile of endothelial cells (ECs) during the dynamic BBB-to-BBTB transition that involves the tumor vessels. A recent study that significantly contributes in this direction was conducted using single-cell RNA sequencing on ECs from human GB, aiming to precisely identify specific genetic profiles and molecular phenotypes. The study demonstrated that although many mRNAs encoding BBB-specific transporters and junctional proteins are still expressed in tumor ECs, gene signatures are highly heterogeneous across GB vessels and differ markedly from those in control brain tissue [26]. The expression of key BBB transporters, including P-glycoprotein (P-gp), is inversely correlated with the expression of genes involved in angiogenesis events and is significantly reduced in tumor core compared to the peripheral tumor areas; in contrast, endothelial genes associated with angiogenic molecules and regulators, including CD146, are upregulated in the tumor core, along with vascular permeability markers [26]. Conversely, genes associated with angiogenic regulators, such as CD146, are upregulated in the tumor core, along with the vascular permeability marker PLVAP [26]. In addition, a number of tumor cell-derived signals promote endothelial dedifferentiation, which is characterized by a reduced expression of endothelial-specific genes, such as CD31, and by the activation of mesenchymal genes encoding fibroblast-specific protein 1 (FSP-1) and α-smooth muscle actin (α-SMA), reflecting the acquisition of a mesenchymal-like phenotype [27]. Among the inducers of epithelial-mesenchymal transition (EMT) is CD146, which promotes a cancer stem cell–like phenotype and enhances cell migration in breast cancer [28].

Within this context, molecules such as P-glycoprotein (P-gp) and CD146 have gained attention as markers of the dynamic heterogeneity of tumor endothelial phenotypes. Notably, they belongs to anticorrelated groups of molecules inversely regulated in endothelial vs. tumor cells, making them potential indicators for monitoring the transition from the BBB to the BBTB, while also unveiling changes occurring within the tumor microenvironment [18, 26–28].

P-gp is the first member of the ATP-biding cassette (ABC) transporters, also known as multidrug resistance protein 1 (MDR1) involved in both physiological protection (e.g., BBB and placental barrier) and acquired multidrug resistance in cancer [29–31]. CD146 (also known as MCAM, S-endo-1, P1H12, and MUC18) was originally identified as a novel endothelial biomarker for angiogenesis in the tumor progression of several malignancies, including hepatocellular carcinoma, where CD146 overexpression promotes self-renewal ability and chemoresistance of cancer cells [32–34]. In the CNS, CD146 coordinates the interplay of ECs and pericytes during BBB development, its expression dynamically shifting from ECs of immature microvessels to pericytes that promote BBB maturation by secreting TGF-β1 [34, 35]. In addition, CD146 has been identified as a mesenchymal cell marker [36, 37]. In brain tumors, it is considered a molecular marker of stemness and glioma aggressiveness, as it is co-expressed by CD133 + glioma stem cells (GSCs) and is significantly upregulated in grade 3 and 4 gliomas, where it contributes to the malignant phenotype of cancer cells [38–40].

In this study, we investigated, by immunohistochemistry and morphometric analysis, the vascular distribution patterns of P-gp and CD146 as markers of the tumor microvascular phenotypes across a series of adult-type diffuse glioma histotypes. In this context, the dual-marker histotype-specific comparative analysis, applied as a status indicator of the BBB-BBTB transition, revealed its potential value as a histopathological grading

criterion. Integrating glioma molecular markers with histopathological features and BBB-BBTB transition analytical data, may thus offer a more refined and biologically relevant classification of adult-type diffuse gliomas.

Methods

Case selection, patients and ethical approval

A total of 22 patients diagnosed with adult-type diffuse gliomas were retrospectively selected for this study. All patients underwent neurosurgical procedures between 2021 and 2023 at the Neurosurgery Unit of the University of Bari "Aldo Moro", Polyclinic Hospital of Bari. Surgical interventions included craniotomy with tumor resection or stereotactic biopsy, with or without the use of intraoperative neuro-navigation systems. Histopathological evaluation was performed at the Pathology Unit of the same institution, and the diagnosis was rendered according to the 5th edition of the World Health Organization Classification of Tumors of the Central Nervous System [1]. All cases were classified as high-grade gliomas, encompassing glioblastoma IDH-wildtype (GB), astrocytoma IDH-mutant grade 4 (ASTR-4), astrocytoma IDH-mutant grade 3 (ASTR-3), and oligodendroglioma IDH-mutant 1p/19q co-deleted grades 3 and 2 (OLIG-3 and OLIG-2). Clinical data including age, sex, medical history, preoperative imaging, treatment regimens, and follow-up outcomes were obtained from the patients' medical records archived at the Neurosurgery Unit. Patient demographics (age, sex, and geographic origin) were not used as inclusion or exclusion criteria. The study protocol was approved by the local ethics committee and conducted in accordance with the principles of the Declaration of Helsinki (1975, and subsequent amendments). All patients provided written informed consent for both diagnostic and research purposes. Details of individual clinical and pathological features are reported in Supplementary Table 1.

Histological and immunohistochemical analyses

All tissue samples were collected and processed at the Pathology Unit and the Human Anatomy and Histology Unit of the University of Bari "Aldo Moro", Polyclinic Hospital of Bari. A total of 22 tumor samples were formalin-fixed and paraffin-embedded using standard protocols. For each case, three serial 4 µm-thick sections were obtained from representative tumor blocks. One section was stained with hematoxylin and eosin for histological evaluation, while the other two were used for immunohistochemical staining to detect the expression of P-glycoprotein (P-gp) and CD146. P-gp immunostaining was performed manually at Anatomy and Histology Unit, Bari University School of Medicine, according to the following protocol: deparaffination by heating slides in a tissue-drying oven for 1 h at 60°C; washing in twice in xylene for 10 min each at room temperature (RT); rehydration in a graded alcohol scale; rinsing in Tris-buffered saline containing 0.025% Triton X-100 (TBS-Tr) (TBS: pH 7.4, Cat. ab64248, Abcam, Cambridge, U.K. Triton X-100: Cat. X100, Merk Life Science S.r.l); antigen retrieval procedure in Dako Target Retrieval Solution (Cat. S1699, Agilent Dako Technologies, Glostrup, Denmark) for 20 min at 96–98°C in thermostatic bath; blocking of endogenous enzyme activity using Dual Endogenous Enzyme-Blocking solution (Cat. S2003, Dako Agilent Technologies) for 10 min at RT; incubation with anti-P-gp monoclonal antibody (1:20; Cat. SIG-38720, clone C494, Signet Laboratories, Dedham, MA, USA) for 30 min at RT; detection with HRP Plus Detection IHC Kit (Cat. ab93697, Abcam) for 10 min at RT followed by 3,3'-Diaminobenzidine DAB Chromogen Kit (Cod. DB801 L, Biocare Medical, Pacheco, CA, USA) for 2 min at RT; nuclear counterstaining with Gill no.1 hematoxylin (Cat. GHS132-1 L, Sigma-Aldrich, Merck KGaA, Darmstadt, Germany). Finally, slides were mounted with Glycergel Aqueous Mounting Medium (Cat. C056330-2, Dako Agilent Technologies). CD146 immunostaining was performed using the Autostainer Link 48 (Dako Agilent, Carpinteria, CA), according to the manufacturer's instructions, at the Pathology Unit, Bari University School of Medicine, according to the following protocol: dewaxing and inhibition of endogenous peroxidase activity (PBS/3% hydrogen peroxide); antigen retrieval with the Envision Flex Target Retrieval Solution High pH in a PT Link Rinse Station (Dako Agilent); incubation with anti-CD146 monoclonal antibody (1:200; Cat. MA5-29413; Thermo Fisher Scientific); detection with EnVision + HRP Labelled Polymer (Dako Agilent) followed by EnVision Flex DAB substrate chromogen (Dako Agilent); nuclear counterstaining with Mayer's hematoxylin. Finally, slides were mounted with Glycergel Aqueous Mounting Medium (Cat. C056330-2, Dako Agilent Technologies). Negative controls were prepared by omitting the primary antibody and mismatching the secondary antibodies. Sections of human placenta and fetal brain were utilized as positive control for both P-gP and CD146. The slides were examined using an Olympus BX60 bright-field microscope at 20× magnification, and subsequently scanned with a NanoZoomer S60 digital scanner (Hamamatsu Photonics) using a 20× objective lens (resulting in 40× digital magnification) to generate a digital archive for downstream image analysis.

Morphometric analysis

A morphometric analysis was performed on the digitally acquired immunostained sections for P-glycoprotein (P-gp) and CD146, scanned using the NanoZoomer S60 digital scanner (Hamamatsu Photonics). The analysis was conducted by two independent observers (G.F. and M.A.), blinded to patient characteristics and group

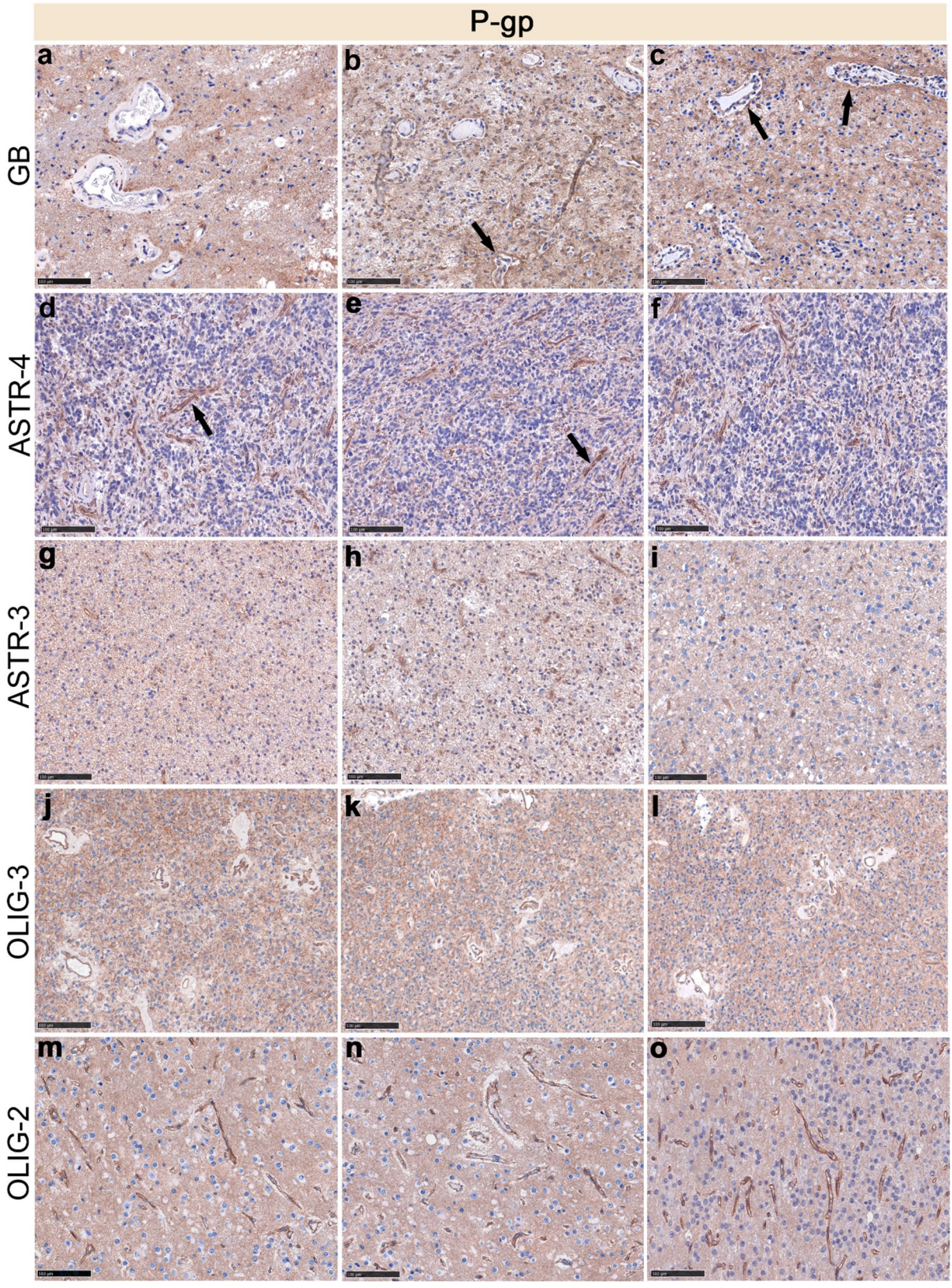


Fig. 1 (See legend on next page.)

(See figure on previous page.)

Fig. 1 Representative images of P-glycoprotein (P-gp) immunolocalization in adult-type diffuse gliomas. Glioblastoma IDH-wildtype (GB), (**a**–**c**); astrocytoma IDH-mutant grade 4 (ASTR-4), (**d**–**f**); astrocytoma IDH-mutant grade 3 (ASTR-3), (**g–i**); oligodendroglioma IDH-mutant, 1p/19q-codeleted, grade 3 (OLIG-3), (**j–l**), and grade 2 (OLIG-2), (**m–o**). P-gp shows strong endothelial expression in non-proliferating vessels of OLIG-2, indicative of a preserved BBB phenotype. This expression progressively decreases with increasing tumor grade, with partial loss in OLIG-3 and ASTR-3, and near-complete loss in proliferating vessels of ASTR-4 and GB. DAB staining, hematoxylin counterstain. Scale bars = 100 µm

allocation of all biopsy specimens, using a semi-automated interactive protocol combining Adobe Photoshop and ImageJ software (NIH, Bethesda, USA). The mean values from the two independent observers were used for quantitative analyses and plotted data. Interobserver agreement was 81.2%. For each patient ($n = 22$), two representative virtual slides—one stained for P-gp and one for CD146—were analyzed. From each slide, four tumor core areas were selected with the support of a neuropathologist (AdA), based on adequate tumor cellularity, absence of artifacts, and exclusion of necrosis, for a total of 8 representative images per patient. Images were acquired at a resolution of 1280 × 1032 pixels (8-bit) and saved in JPEG format. The image processing workflow included the following steps (see Supplementary Fig. 2 for a visual example):

1. Image preparation: Each image was opened in Adobe Photoshop, and key microanatomical structures were manually identified using the free-hand selection tool. These included: (i) proliferating and non-proliferating microvessels (the evaluation was performed by a neuropathologist (AdA), who identified proliferating vessels by features such as multilayered endothelial cells, glomeruloid structures, or endothelial hyperplasia, in contrast to thin-walled, non-proliferating capillaries, according to WHO-defined morphological criteria routinely used in the diagnostic evaluation of CNS tumors [1]); (ii) endothelial lining; (iii) thickened walls of hypertrophic vessels; and (iv) surrounding tumor tissue.
2. Cropping and color adjustment: Selected regions were cropped and saved as individual JPEG files. A color thresholding process was then applied to isolate DAB-positive staining, using the following path: Image > Adjust > Replace Color. Nuclear hematoxylin counterstain (violet-blue) was removed to improve contrast.
3. Grayscale conversion and optimization: Images were converted to grayscale and further adjusted for brightness (50) and contrast (80).
4. Quantification: Processed images were imported into ImageJ, where the Area Fraction tool (under the Analyze menu) was used to calculate the percentage of positive pixel area (area % on the total image area) corresponding to immunoreactive signal in each region.

This approach allowed for semi-quantitative assessment of marker expression in the tumor vasculature, minimizing operator bias while retaining spatial context.

Statistical analysis

Comparisons between groups were performed using one-way ANOVA followed by Bonferroni's multiple comparison test, performed using GraphPad Prism (release 6.0, GraphPad Software, La Jolla, USA). The plots showed both single patient mean values and mean value for each tumor histotype. Differences were considered statistically significant at a p-value of < 0.05.

Results

Clinical, radiological and pathological features

Clinical, radiological, and surgical data were retrospectively collected from institutional records (Supplementary Table 1). All patients underwent preoperative brain imaging by CT and/or MRI, allowing assessment of tumor localization, necrotic core, peritumoral edema, and contrast enhancement. Histopathological and molecular classifications followed the 2021 WHO CNS criteria and are reported in Supplementary Table 1.

Immunohistochemical characterization of P-glycoprotein (P-gp) and CD146 expression patterns

To investigate the phenotypic transition of glioma vasculature from blood–brain barrier (BBB) to blood–brain tumor barrier (BBTB), we performed an extensive qualitative evaluation of P-gp and CD146 immunoreactivity in endothelial and tumor compartments, across glioma histotypes.

P-gp immunolocalization and patterns of distribution across glioma histotypes (Supplementary table 1)

Glioblastoma, IDH-wildtype (GB, n = 9) In glioblastomas (GB, $n = 9$), a diffuse granular cytoplasmic positivity for P-gp was consistently detected in tumor cells. Moreover, in over half of the cases (55.5%), perivascular tumor cells exhibited focal P-gp positivity, suggesting an involvement of perivascular niches in drug resistance. The staining for P-gp in endothelial cells of proliferating vessels was generally weak or absent: five cases (55.5%) showed focal abluminal expression, while three were completely negative and only one case retained endothelial immunoreactivity. Conversely, P-gp positivity in non-prolifer-

ating vessel endothelium was preserved in 44.4% of cases (Fig. 1a-c).

Astrocytoma, IDH-mutant, grade 4 (ASTR-4, n = 4) Astrocytomas grade 4 (ASTR-4, $n = 4$) also displayed diffuse P-gp immunostaining in tumor cells in three cases, with one case showing a biphasic glial/neuronal phenotype, the glial component being P-gp positive. All four tumors showed P-gp reactivity in endothelial cells of non-proliferating vessels, while 75% retained expression in proliferating vessels (Fig. 1d-f).

Astrocytoma, IDH-mutant, grade 3 (ASTR-3, n = 3) In ASTR-3 ($n = 3$), P-gp was expressed in tumor cells and endothelial cells of non-proliferating vessels, in keeping with the absence of MVPs in this histotype (Fig. 1g-i).

Oligodendroglioma, IDH-mutant, 1p/19q-codeleted, grade 3 (OLIG-3, n = 3) Only one case exhibited P-gp expression in neoplastic and endothelial cells; two cases completely lacked neoplastic and endothelial cell P-gp expression. All three tumors showed P-gp positivity in non-proliferating vessel endothelium (Fig. 1j-l).

Oligodendroglioma, IDH-mutant, 1p/19q-codeleted, grade 2 (OLIG-2, n = 3) No P-gp positivity was detected in tumor cells. However, all samples showed consistent P-gp immunostaining of endothelial cells of non-proliferating vessels (Fig. 1m-o).

CD146 immunolocalization and patterns of distribution across glioma histotypes (Supplementary table 1)

Glioblastoma, IDH-wildtype (GB, n = 9) All tumors demonstrated strong CD146 reactivity in endothelial cells of both proliferating and non-proliferating vessels. Six cases (66.6%) exhibited CD146-positive tumor cells, including single neoplastic elements with gemistocytic morphology and multinucleated giant cells, which displayed complex branching processes (Fig. 2a–c).

Astrocytoma, IDH-mutant, grade 4 (ASTR-4, n = 4) CD146 immunostaining appeared diffuse in both tumor and endothelial compartments (Fig. 2d–f). Notably, the biphasic case showed CD146 immunoreactivity in both glial and neuronal components, although with a more focal pattern in the latter.

Astrocytoma, IDH-mutant, grade 3 (ASTR-3, n = 3) Diffuse CD146 staining was observed in tumor cells, with scattered CD146-positive gemistocytes in one case (33%). Endothelial positivity was restricted to non-proliferating vessels (Fig. 2g–i).

Oligodendroglioma, IDH-mutant, 1p/19q-codeleted, grade 3 (OLIG-3, n = 3) All tumors were positive for CD146 in tumor cells, with stronger staining in areas with anaplastic features. Endothelial CD146 staining was observed in both vessel types (Fig. 2j–l).

Oligodendroglioma, IDH-mutant, 1p/19q-codeleted, grade 2 (OLIG-2, n = 3) Tumor cells were negative for CD146 in all cases. Endothelial positivity was limited to proliferating vessels (Fig. 2m–o).

Morphometric quantitative analyses

P-gp expression by morphometric evaluation

Endothelial cells (ECs) Morphometric analysis confirmed a striking histotype-specific pattern. The 'Area Fraction' (AF) parameter, expressed as area % of P-gp$^+$ ECs (on total image area), was highest in OLIG-2 (2.96 ± 0.11%), significantly exceeding all other groups: GB (0.56 ± 0.27%), ASTR-4 (0.73 ± 0.19%), ASTR-3 (0.51 ± 0.37%), and OLIG-3 (0.54 ± 0.41%). These differences were statistically significant (OLIG-2 vs. GB, $p < 0.0001$; OLIG-2 vs. others, $p < 0.01$) (Fig. 3a), suggesting preserved expression of the BBB efflux transporter P-gp in OLIG-2 tumors, with a progressive loss in more aggressive gliomas.

Hypertrophied thickened vessel walls An opposite trend was observed in the thickened vessel walls of MVPs. GB showed the highest P-gp AF (0.27 ± 0.11%), significantly greater than ASTR-4 (0.04 ± 0.04%) and OLIG-3 (0.09 ± 0.07%) (GB vs. ASTR-4, $p < 0.05$) (Fig. 3b). This pattern likely reflects the accumulation of multidrug-resistant cancer cells (MDR-CCs) in perivascular regions.

Extravascular tissue (EVT) Tumor cell expression of P-gp in EVT was most prominent in GB (8.29 ± 2.02%), followed by OLIG-3 (3.65 ± 3.42%), ASTR-3 (2.86 ± 3.68%), and ASTR-4 (2.61 ± 2.48%). OLIG-2 was completely negative. GB vs. OLIG-2 reached statistical significance ($p < 0.0001$), as did GB vs. ASTR-4 ($p < 0.05$) (Fig. 3c).

CD146 expression by morphometric evaluation

Endothelial cells (ECs) CD146 expression was proportional to tumor grade. Endothelial CD146 expression was highest in GB (0.93 ± 0.26%), followed by OLIG-3 (0.70 ± 0.36%) and ASTR-4 (0.63 ± 0.54%), with significantly lower values in ASTR-3 (0.29 ± 0.13%) and OLIG-2 (0.23 ± 0.006%) (GB vs. ASTR-3, $p < 0.001$; GB vs. OLIG-2, $p < 0.0001$) (Fig. 3d).

Hypertrophied thickened vessel walls CD146 positivity was highest in ASTR-4 (0.12 ± 0.07%), while GB (0.04 ± 0.04%) and OLIG-3 (0.003 ± 0.006%) showed lower

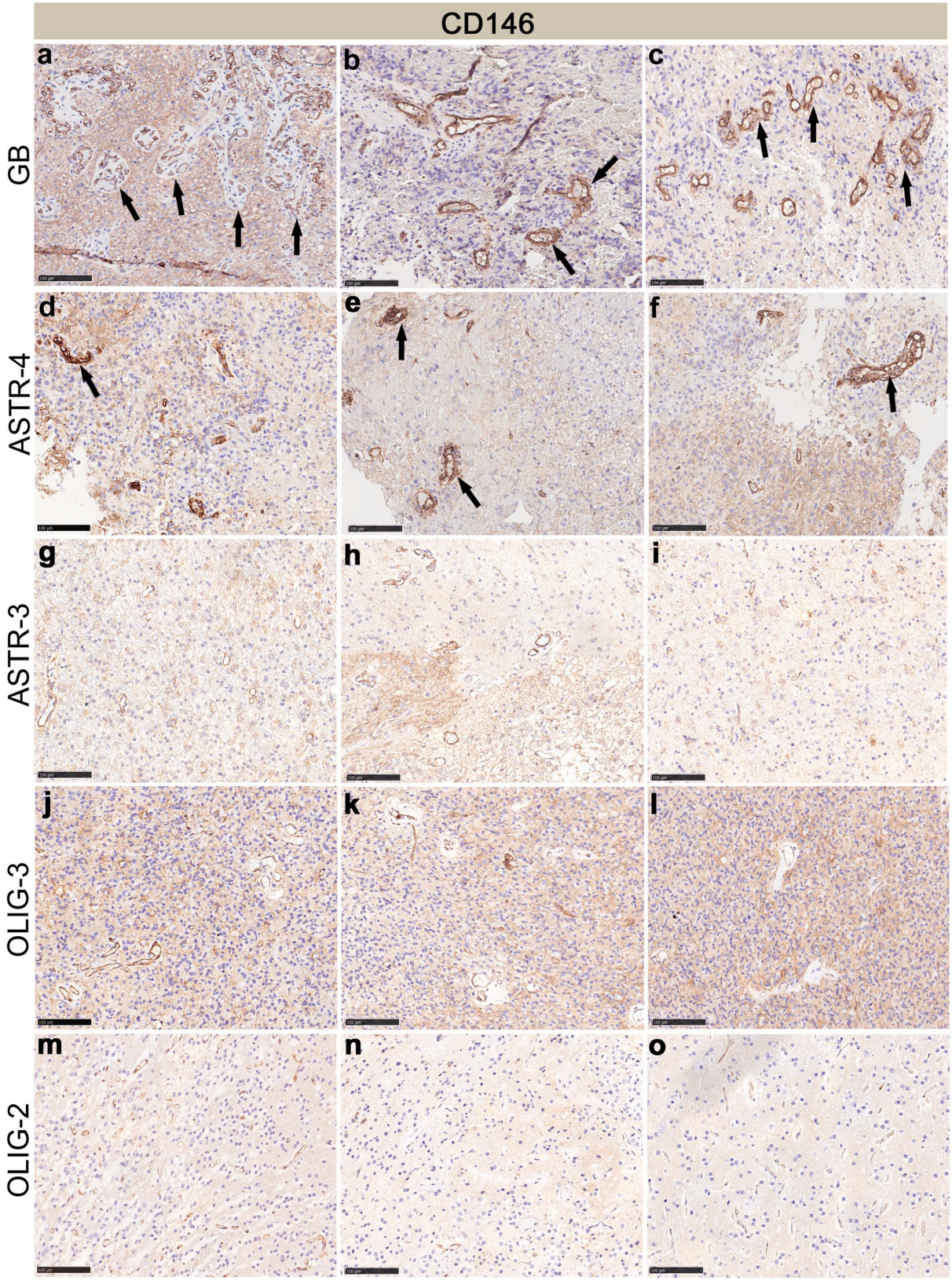


Fig. 2 Representative images of CD146 immunolocalization in adult-type diffuse gliomas. Glioblastoma IDH-wildtype (GB), (**a**–**c**); astrocytoma IDH-mutant grade 4 (ASTR-4), (**d**–**f**); astrocytoma IDH-mutant grade 3 (ASTR-3), (**g**–**i**); oligodendroglioma IDH-mutant, 1p/19q-codeleted, grade 3 (OLIG-3), (**j**–**l**), and grade 2 (OLIG-2), (**m**–**o**). CD146 expression increases with malignancy: it is virtually absent in OLIG-2, limited in OLIG-3 and ASTR-3, and prominent in GB and ASTR-4, involving both endothelial and tumor compartments. DAB staining, hematoxylin counterstain. Scale bars = 100 µm

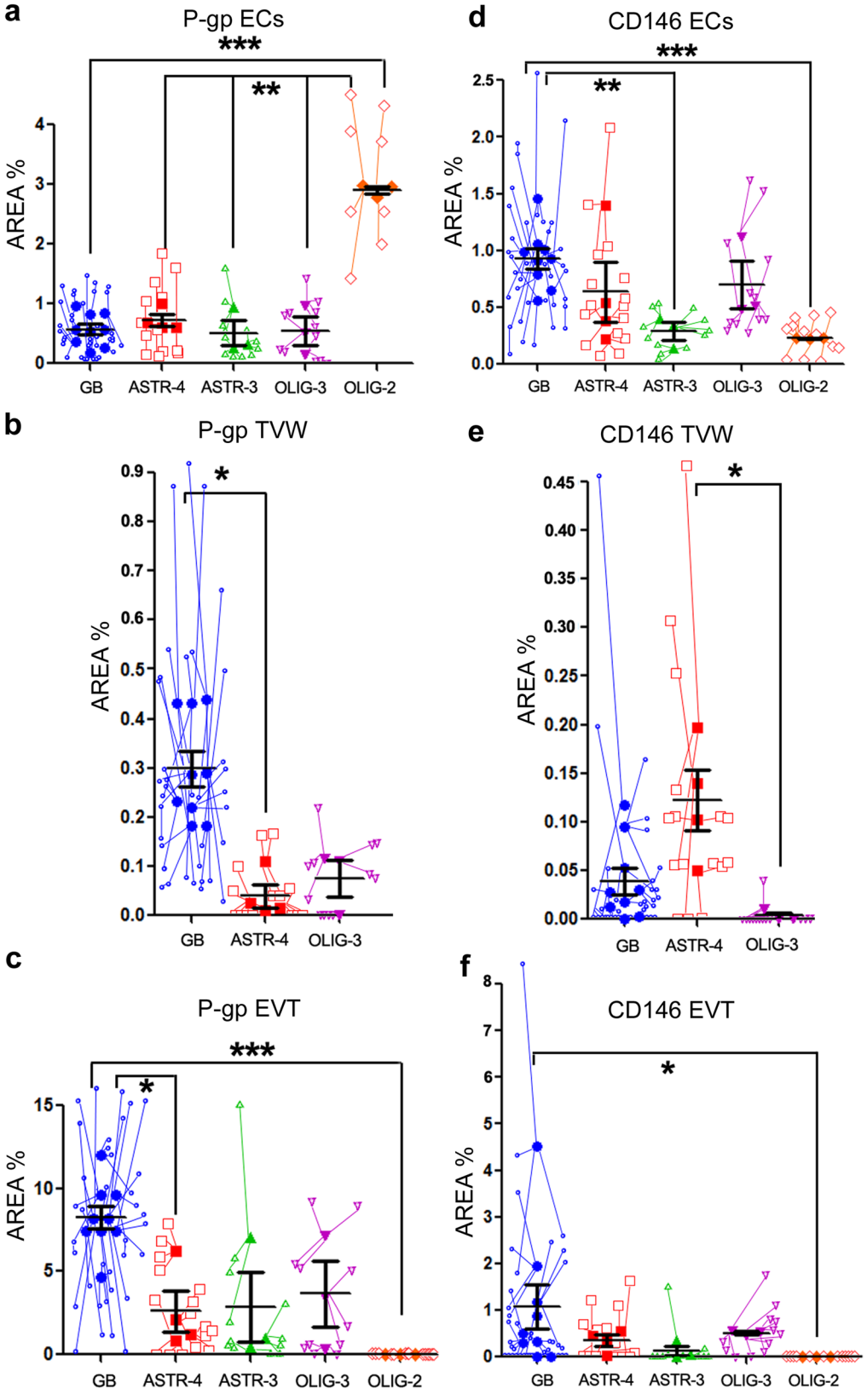


Fig. 3 (See legend on next page.)

(See figure on previous page.)

Fig. 3 Semi-quantitative morphometric analysis of P-glycoprotein (P-gp) and CD146 immunoreactivity across different glioma histotypes. Plot graphs represent the percentage of immunoreactive area (area %) for P-gp (**a**–**c**) and CD146 (**d**–**f**), assessed in three distinct tissue compartments: (**a**, **d**) endothelial cells (ECs) of non-proliferating vessels; (**b**, **e**) thickened vessel walls (TVW) of microvascular proliferations; and (**c**, **f**) extravascular tumor tissue (EVT). The empty points represent the four tumor areas connected to the mean individual patient; the horizontal black lines represent the mean ± SD of the overall groups (GB: glioblastoma IDH-wildtype; ASTR-4 and ASTR-3: astrocytoma IDH-mutant grade 4 and 3; OLIG-3 and OLIG-2: oligodendroglioma IDH-mutant, 1p/19q-codeleted, grade 3 and 2). OLIG-2 displays the highest endothelial P-gp expression and the lowest CD146 levels, consistent with a preserved BBB phenotype. In contrast, GB and ASTR-4 exhibit reduced endothelial P-gp and increased CD146 expression, reflecting BBB-to-BBTB transition. P-gp + elements are enriched in the vessel walls of GB, while CD146 + cells predominate in the same region of ASTR-4. GB also shows the highest combined expression of P-gp and CD146 in the tumor parenchyma, indicating coexisting therapy-resistant and stem-like subpopulations. Statistical analysis was performed using one-way ANOVA followed by Bonferroni's multiple comparison test. $N = 22$. $^{*}p < 0.05$, $^{**}p < 0.01$, $^{***}p < 0.0001$

levels. The difference between ASTR-4 and OLIG-3 was significant ($p < 0.05$) (Fig. 3e).

Extravascular tissue (EVT) CD146 expression in neoplastic EVT was highest in GB (1.07 ± 1.43%), followed by OLIG-3 (0.51 ± 0.06%), ASTR-4 (0.37 ± 0.22%), and ASTR-3 (0.13 ± 0.19%). OLIG-2 was consistently negative. GB vs. OLIG-2: $p < 0.05$ (Fig. 3f).

Dual-marker comparative analysis: P-gp vs. CD146

A comparative evaluation of P-gp and CD146 expression in endothelial cells, vessel wall, and tumor parenchyma further underscored the dynamic transition from a blood–brain barrier (BBB)-like to a blood–brain tumor barrier (BBTB)-like phenotype in adult-type diffuse gliomas. This analysis revealed tumor-specific profiles, reflecting not only the grade of malignancy, but also the extent of endothelial differentiation, vascular remodeling, and the presence of stem-like or therapy-resistant cellular subpopulations. (Fig. 3 and Supplementary Figs. 3, 4).

Endothelial cells (ECs) In the microvascular endothelium, a clear inverse pattern emerged between OLIG-2 and GB. Oligodendrogliomas grade 2 demonstrated high P-gp expression and minimal CD146 immunoreactivity, consistent with a preserved BBB phenotype. The statistical comparison confirmed a significant difference between P-gp and CD146 expression levels in this group ($p < 0.0001$) (Fig. 3 and Supplementary Figs. 3, 4), supporting the interpretation of a mature, functionally intact microvascular compartment. In contrast, glioblastomas displayed the opposite configuration, with high CD146 expression and reduced P-gp levels ($p < 0.05$) (Fig. 3 and Supplementary Figs. 3, 4), indicative of a phenotypic shift toward immature, mesenchymal-like endothelial cells associated with BBB disruption. Interestingly, astrocytoma grade 3 (ASTR-3) exhibited an intermediate profile, with moderately low levels of both markers and a slight predominance of CD146 over P-gp according to the high tumor grade (Fig. 3 and Supplementary Figs. 3, 4). These findings delineate a molecular continuum of endothelial transformation that parallels histological grading, with OLIG-2 and GB representing opposite poles of the spectrum, and ASTR-3 situated in a transitional state.

Hypertrophied thickened vessel wall (TVW) In the thickened vessel wall of microvascular proliferations (MVPs), the spatial distribution of P-gp and CD146 positive cells revealed tumor-specific infiltration patterns. In glioblastoma, thickened vascular walls harbored a substantial population of P-gp-positive cells, significantly outnumbering CD146-positive elements ($p < 0.05$) (Fig. 3 and Supplementary Figs. 3, 4). This finding may reflect the accumulation of multidrug-resistant cancer cells (MDR-CCs) in perivascular niches, a hallmark of GB aggressiveness. A similar predominance of P-gp positive infiltrating cells was observed in OLIG-3, although at lower overall expression levels. Conversely, in ASTR-4, CD146 positive cells were more frequently detected in MVP walls, with a significantly higher representation than in OLIG-3 ($p < 0.05$) (Fig. 3 and Supplementary Figs. 3, 4). Notably, ASTR-4 retained a small population of P-gp reactive cells, suggesting the coexistence of two distinct tumor subpopulations within the perivascular microenvironment. The presence of these divergent cell types - P-gp + in GB, CD146 + in ASTR-4 - may represent a histotype-specific infiltration pattern, potentially useful as a diagnostic adjunct in high-grade gliomas.

Extravascular tissue (EVT) In the extravascular tumor tissue (EVT), the expression of P-gp and CD146 further reinforced the distinction between high- and low-grade gliomas. OLIG-2 consistently lacked both markers, aligning with its low aggressiveness and suggesting the absence of multidrug-resistant or stem-like cancer cells in the tumor parenchyma. In contrast, glioblastomas exhibited markedly high expression of both P-gp (8.29 ± 2.02%) and CD146 (1.07 ± 1.43%) in neoplastic cells, with a statistically significant predominance of P-g positive elements ($p < 0.05$) (Fig. 3 and Supplementary Figs. 3, 4). These findings also suggest the coexistence of two functionally distinct subpopulations: one associated with drug efflux and chemoresistance (P-gp+), the other with stemness and cellular plasticity (CD146+). A similar, although less pronounced, dual expression profile was observed in ASTR-4 and ASTR-3, where both markers were expressed at intermediate levels, although, according to tumor degree, in ASTR-3 CD146 was consistently lower compared with ASTR-4 ($p < 0.0001$) (Fig. 3 and Supplementary Figs. 3,

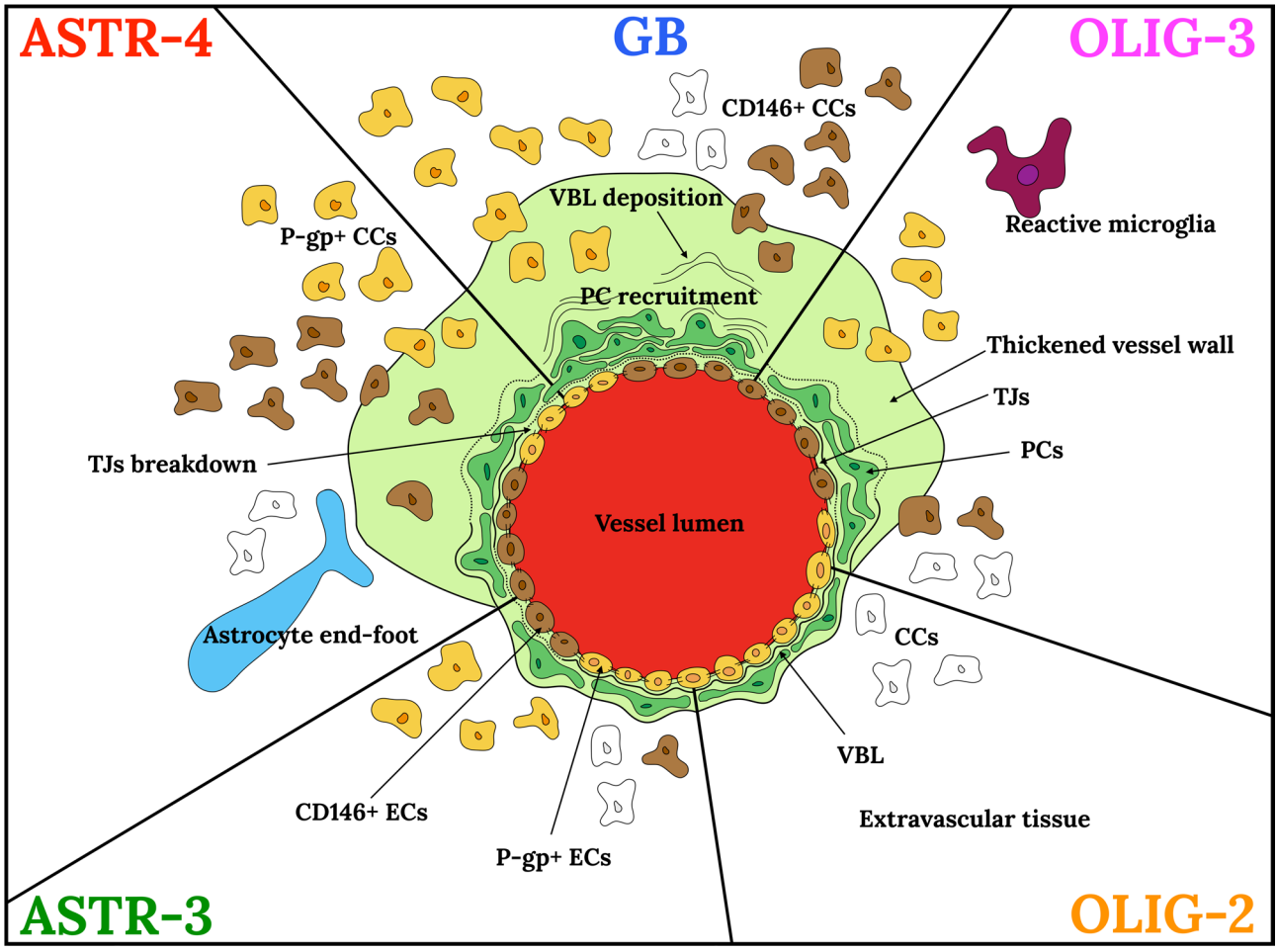


Fig. 4 Schematic representation of the main findings of this study, showing how P-gp/CD146 dual-marker expression reflects glioma histotype-specific features and the main changes that settle the transition to a blood-brain tumor barrier. Glioblastoma IDH-wildtype (GB), astrocytoma IDH-mutant grade 4 (ASTR-4), astrocytoma IDH-mutant grade 3 (ASTR-3), oligodendroglioma IDH-mutant, 1p/19q-codeleted, grade 3 (OLIG-3), and grade 2 (OLIG-2). P-gp immunostaining in yellow and CD146 immunostaining in brown; ECs, endothelial cells; PCs, pericytes; CCs, cancer cells; VBL, vessel basal lamina; TJs, Tight junctions

4), again suggesting a bias toward therapy resistance and stemness features in higher tumor grades. In OLIG-3, although at lower levels, P-gp + elements were more frequent than CD146 + cells indicating a potentially more prominent role for chemoresistance than for stem-like characteristics.

Taken together, the co-analysis of P-gp and CD146 expression across multiple tumor compartments revealed a robust inverse correlation at the endothelial level and a complex coexistence in tumor cells and perivascular regions. This dual-marker approach provides a refined understanding of the BBB–BBTB transition and identifies distinct microvascular and neoplastic profiles that correlate with glioma histotype and grade. To illustrate and integrate the findings presented above, a graphical summary is shown in Fig. 4.

Discussion

The present study investigates the endothelial phenotype across a spectrum of adult-type diffuse gliomas by analyzing the expression of two vascular markers, P-glycoprotein (P-gp) and CD146, using both qualitative and morphometric approaches. These markers were selected for their complementary roles: P-gp as a canonical efflux transporter associated with blood–brain barrier (BBB) integrity and multidrug resistance, and CD146 as a cell adhesion molecule linked to endothelial plasticity and tumor progression [13, 29, 32–34, 37, 41]. Our results reveal histotype-specific and spatially distinct expression patterns of both markers, reflecting a progressive shift from BBB-like to blood–brain tumor barrier (BBTB)-like microvasculature in correlation with glioma grade.

P-gp expression was predominantly retained in the endothelium of non-proliferating vessels within low-grade gliomas, especially oligodendroglioma grade 2

(OLIG-2), and progressively diminished in higher-grade tumors such as glioblastoma (GB) and astrocytoma grade 4 (ASTR-4). These findings are consistent with previous evidence indicating that P-gp is a hallmark of mature BBB endothelium and is progressively lost during barrier disruption [13, 29, 42, 43]. In contrast, CD146 expression was highest in high-grade gliomas, where it was observed in both endothelial and extravascular compartments, notably within proliferating vessels and tumor cell niches. This upregulation aligns with the recognized role of CD146 in promoting angiogenesis, mesenchymal transition, and treatment resistance in malignant gliomas [41, 44, 45].

The morphometric data corroborates the immunohistochemical observations, demonstrating that P-gp expression (quantified as area fraction) in endothelial cells was significantly higher in OLIG-2 than in GB, ASTR-4, and other histotypes, supporting the hypothesis of preserved BBB function in low-grade tumors. Conversely, CD146 endothelial expression increased with tumor grade and was particularly elevated in GB and OLIG-3, suggesting that CD146 may act as a surrogate marker of BBTB formation and vascular dedifferentiation. Notably, both markers also exhibited expression in extravascular tumor areas, particularly in high-grade gliomas, further supporting their relevance in tumor cell biology beyond endothelial phenotyping.

These findings offer novel insights into the histopathological continuum of BBB–BBTB transition, which has been traditionally inferred from radiological or ultrastructural data but poorly characterized at the immunophenotypic level. Our data expand on previous studies that describe heterogeneous BBB disruption in gliomas [31], showing that distinct endothelial molecular profiles can be identified even within the same tumor grade, potentially refining current grading criteria. Indeed, while conventional histological parameters such as microvascular proliferation (MVP) and necrosis remain essential for diagnosis, they do not fully capture the functional and molecular heterogeneity of the tumor vasculature [6, 19, 21].

The implications of our findings are both diagnostic and translational. From a diagnostic standpoint, the dual-marker approach using P-gp and CD146 may serve as an adjunct tool for glioma grading, particularly in borderline or histologically ambiguous cases. Moreover, as both markers are involved in therapeutic resistance—P-gp by limiting chemotherapeutic penetration, and CD146 through modulation of radiotherapy resistance and invasive potential—they represent potential targets for vascular-directed therapies [41, 44, 45]. The integration of these markers in routine immunohistochemical panels may therefore aid in stratifying patients for individualized therapeutic regimens, including drug delivery strategies that bypass intact BBB regions or inhibit specific components of the tumor vasculature.

However, this study is not without limitations. The sample size, though larger than previous pilot studies, remains modest ($n = 22$), and the retrospective design may introduce selection bias. While morphometric analysis was semi-quantitative and blinded, it was limited to predefined regions of interest and did not account for intratumoral spatial heterogeneity in full three-dimensional context. Furthermore, molecular data regarding MGMT methylation status, EGFR amplification, or CDKN2A/B deletion were not uniformly available and thus could not be correlated with marker expression. Future studies incorporating larger, multicenter cohorts and integrated molecular profiling are warranted to validate the prognostic and predictive value of these vascular markers.

In conclusion, our study highlights the potential of P-gp and CD146 as complementary endothelial markers delineating the BBB–BBTB continuum in adult-type diffuse gliomas. Their differential expression according to histotype and grade reflects underlying vascular remodeling processes and may inform both diagnostic classification and therapeutic targeting. Expanding the application of vascular immunophenotyping in neuropathology could improve the granularity of glioma characterization and ultimately support the development of barrier-specific interventions in neuro-oncology.

Supplementary Information

The online version contains supplementary material available at https://doi.org/10.1186/s12987-025-00707-z.

Supplementary Material 1: Table 1. Additional data overview by patient's characteristics, clinical and radiological results, P-gp and CD146 patterns of expression based on microscopical analyses. The 22 cases have been named as follows: patient 1 to patient 9 with a diagnosis of Glioblastoma, *IDH*-wildtype (GBM n.1 to GBM n. 9); patient 1 to patient 4 with a diagnosis of Astrocytoma, *IDH*-mutant, CNS WHO grade 4 (ASTR-4 n.1 to ASTR-4 n.4); patient 1 to patient 3 with a diagnosis of Astrocytoma, *IDH*-mutant, CNS WHO grade 3 (ASTR-3 n.1 to ASTR-3 n.3), patient 1 to patient 3 with a diagnosis of Oligodendroglioma, *IDH*-mutant, 1p/19q-codeleted, CNS WHO grade 3 (OLIG-3 n.1 to OLIG-3 n.3); patient 1 to patient 3 with a diagnosis of Oligodendroglioma, *IDH*-mutant, 1p/19q-codeleted, CNS WHO grade 2 (OLIG-2 n.1 to OLIG-2 n.3). Abbreviations referring to patient's characteristic : Male = M; Female = F; Frontal lobe = F; Parietal lobe = P; Temporal lobe = T; Occipital lobe = O; Corpus Callosum = C.C.; Cerebellum = C; Stereotactic biopsy with neuro-navigation = S.B. w/ N.; Craniotomy and tissue removal with neuro-navigation = C and T.R.; Open biopsy = O. B.; PFS = Progression-Free Survival, here defined as the time from the surgical intervention to the death of the patient ; * = patient still alive at the time of this study; ** = patient died during the neurosurgical operation. PFS = Progression Free Survival (counted from the day of operation till death). * = patient still alive at the time of this study; ** = death at the time of the surgical operation; / = radiological information not available at the time of this study. Abbreviation referring to clinical and pathological results: Mvp = microvascular proliferation; / = no data found. Abbreviation referring to P-gp and CD146 patterns of expression: * = possibly represented by a residual expression of P-gp on the basolateral endothelial plasma membrane.

Supplementary Material 2: Figure 1. CNS WHO 2021 Classification on adult-

type diffuse gliomas: steps for a precise diagnosis. The term microvascular proliferations (MVP, in red) identifies the morphological types and subtypes of neo-formed microvessels that characterize the highly vascularized histotypes.

Supplementary Material 3: Figure 2. Morphometric analysis. An example of image processing based on the descripted thresholding method and applied to a P-gp immunostained section of GB. A and B: open image with Adobe Photoshop and select an area to measure; C, D, E: identify and select using the free-hand tool the vessel endothelial lining (C), the thickened wall of hypertrophic vessels (D), and the remaining tissue (E); 1, 2, 3, 4: thresholding method – 1: "image" / "adjust" / "color replacement" / remove the nuclear violet-blue color, 2: "method" / "gray scale", 3: "brightness and contrast" (values 50 "brightness" and 80 "contrast". The measuring method was carried out with ImageJ software in order to calculate the %Fraction Area of the threshold black pixeled dots obtained on each image in step 4.

Supplementary Material 4: Figure 3. Immunohistochemical expression of P-glycoprotein (P-gp, left column) and CD146 (right column) in adult-type diffuse gliomas, from the same tumor area and adjacent sections. (a, b) glioblastoma IDH-wildtype (GB), (c, d) astrocytoma IDH-mutant grade 4 (ASTR-4), (e-f) astrocytoma IDH-mutant grade 3 (ASTR-3), (g-h) oligodendroglioma IDH-mutant, 1p/19q-codeleted, grade 3 (OLIG-3), and (i, j) grade 2 (OLIG-2). P-gp shows strong expression in non-proliferating vessels of OLIG-2, indicative of a preserved endothelial BBB phenotype. The endothelial P-gp staining progressively decreases with increasing tumor grade, until its near-complete loss in proliferating vessels of ASTR-4 and GB. Conversely, the endothelial CD146 staining increases with malignancy: it is virtually absent in OLIG-2 and prominent in GB and ASTR-4. A parallel increase is observed in the extravascular tumor areas, except for Astr-3, that shows a limited or absent CD146 tissue staining. These opposing expression patterns shown by the dual marker comparative analysis reflect a histotype-specific shift from BBB-like to BBTB-like microvascular phenotypes. DAB staining, hematoxylin counterstain. Scale bars = 100 µm.

Supplementary Material 5: Figure 4. Immunohistochemical expression of P-glycoprotein (P-gp, left column) and CD146 (right column) in non-tumoral tissue from samples of astrocytoma IDH-mutant grade 4 (ASTR-4; a, b) and oligodendroglioma IDH-mutant, 1p/19q-codeleted, grade 3 (OLIG-3; c, d). The strong P-gp staining of endothelial cells of normal brain vessels (a, b) is in contrast with the absence of endothelial CD146 immunostaining on sections from the same glioma histotypes (b, d). Scale bars = 100 µm.

Author contributions
A.M. and F.G. performed immunohistochemical and morphometric analyses, interpreted data, and contributed equally to manuscript drafting.A.Mz., M.D.G. and T.A. assisted with histological evaluations and clinical data collection.R.M. and F.S. contributed to the acquisition and analysis of radiological and surgical data.A.d'A. and G.I. provided pathological supervision and critical review of the methodology.D.V. contributed to the conceptualization of the study and scientific oversight.M.E. and A.d'A. conceived the project, designed the study, supervised the entire work, and contributed equally to writing and revising the manuscript.All authors reviewed and approved the final manuscript.

Funding
No funding has been received for this study.

Data availability
No datasets were generated or analysed during the current study.

Declarations

Ethics approval and consent to participate
This retrospective study was approved by the local Ethics Committee of the University of Bari (no study number was assigned, due to the retrospective nature of the study). It was conducted according to the Declaration of Helsinki in its applicable version. Tissue samples were collected from the archive of the Anatomical Pathology Unit, and previously obtained during surgery at the Neurosurgery Unit, of University of Bari. All patients provided informed consent, for diagnostic and therapeutic procedures, as well as for the potential use of biological samples for research purposes.

Consent for publication
All authors gave their consent for publication.

Competing interests
The authors declare no competing interests.

Author details
[1]Department of Translational Biomedicine and Neuroscience (DiBraiN), Human Anatomy and Histology Unit, University of Bari School of Medicine, Bari, Italy
[2]Section of Anatomical Pathology, Department of Precision and Regenerative Medicine and Ionian Area (DiMePRe-J), University of Bari School of Medicine, Bari, Italy
[3]Department of Medicine and Surgery, LUM University, Casamassima, Bari, Italy
[4]Department of Translational Biomedicine and Neuroscience (DiBraiN), Division of Neurosurgery, University of Bari School of Medicine, Bari, Italy
[5]Anatomical Pathology Unit, Fondazione Policlinico Universitario "A. Gemelli" IRCCS, Università Cattolica S. Cuore, Rome, Italy

Received: 23 May 2025 / Accepted: 2 September 2025
Published online: 01 October 2025

References
1. WHO Classification of Tumours Editorial Board. Central nervous system tumours. Lyon (France): International Agency for Research on Cancer; 2021. (WHO classification of tumours series, 5th ed.; vol. 6). https://publications.iarc.fr/601.
2. Wang W, Zhao Y, Teng L, Yan J, Guo Y, Qiu Y, et al. Neuropathologist-level integrated classification of adult-type diffuse gliomas using deep learning from whole-slide pathological images. Nat Commun. 2023;14:6359.
3. Louis DN, Perry A, Wesseling P, Brat DJ, Cree IA, Figarella-Branger D, et al. The 2021 WHO classification of tumors of the central nervous system: a summary. Neuro Oncol. 2021;23:1231–51.
4. Gupta S, Nawabi NL, Emani S, Medeiros L, Bernstock JD, Duvall J, et al. An expanded role for surgery in grade 3 1p/19q co-deleted oligodendroglioma. Neuro-Oncology Adv. 2023;5:vdad046.
5. Carstam L, Latini F, Solheim O, Bartek J, Pedersen LK, Zetterling M, et al. Long-term follow up of patients with WHO grade 2 oligodendroglioma. J Neurooncol. 2023;164:65–74.
6. Chen L, Lin Z-X, Lin G-S, Zhou C-F, Chen Y-P, Wang X-F, et al. Classification of microvascular patterns via cluster analysis reveals their prognostic significance in glioblastoma. Hum Pathol. 2015;46:120–8.
7. Kadry H, Noorani B, Cucullo L. A blood–brain barrier overview on structure, function, impairment, and biomarkers of integrity. Fluids Barriers CNS. 2020;17:69.
8. Virgintino D, Monaghan P, Robertson D, Errede M, Bertossi M, Ambrosi G, et al. An immunohistochemical and morphometric study on astrocytes and microvasculature in the human cerebral cortex. Histochem J. 1997;29:655–60.
9. Rojiani AM, Dorovini-Zis K. Glomeruloid vascular structures in glioblastoma multiforme: an immunohistochemical and ultrastructural study. J Neurosurg. 1996;85:1078–84.
10. Alajangi HK, Kaur M, Sharma A, Rana S, Thakur S, Chatterjee M, et al. Blood–brain barrier: emerging trends on transport models and new-age strategies for therapeutics intervention against neurological disorders. Mol Brain. 2022;15:49.
11. Sarkaria JN, Hu LS, Parney IF, Pafundi DH, Brinkmann DH, Laack NN, et al. Is the blood-brain barrier really disrupted in all glioblastomas? A critical assessment of existing clinical data. Neuro Oncol. 2018;20:184–91.
12. Ishihara H, Kubota H, Lindberg RLP, Leppert D, Gloor SM, Errede M, et al. Endothelial cell barrier impairment induced by glioblastomas and transforming growth factor beta2 involves matrix metalloproteinases and tight junction proteins. J Neuropathol Exp Neurol. 2008;67:435–48.
13. de Trizio I, Errede M, d'Amati A, Girolamo F, Virgintino D. Expression of P-gp in Glioblastoma: What we can Learn from Brain Development. Curr Pharm Des. 2020;26(13):1428–1437. https://doi.org/10.2174/1381612826666200318130625. PMID: 32186270.

14. Tamma R, Ingravallo G, Annese T, d'Amati A, Lorusso L, Ribatti D. Tumor microenvironment and microvascular density in human glioblastoma. Cells. 2023;12:11.
15. d'Amati A, Bargiacchi L, Rossi S, Carai A, Bertero L, Barresi V, et al. Pediatric CNS tumors and 2021 WHO classification: what do oncologists need from pathologists? Front Mol Neurosci. 2024;17:1268038.
16. d'Amati A, Nicolussi A, Miele E, Mastronuzzi A, Rossi S, Gianno F, et al. NSD1 mutations and pediatric High-Grade gliomas: A comparative genomic study in primary and recurrent tumors. Diagnostics (Basel). 2022;13:78.
17. d'Amati A, Gianno F, Scuccimarri L, Lastilla M, Messina R, Signorelli F, et al. Intracranial mesenchymal tumor with (novel) COX14::PTEN rearrangement. Acta Neuropathol Commun. 2023;11:95.
18. Annese T, Errede M, d'Amati A, De Giorgis M, Lorusso L, Tamma R, et al. Differential P-Glycoprotein/CD31 expression as markers of vascular Co-Option in primary central nervous system tumors. Diagnostics (Basel). 2022;12:3120.
19. Thomsen MS, Routhe LJ, Moos T. The vascular basement membrane in the healthy and pathological brain. J Cereb Blood Flow Metab. 2017;37:3300–17.
20. Knox EG, Aburto MR, Clarke G, Cryan JF, O'Driscoll CM. The blood-brain barrier in aging and neurodegeneration. Mol Psychiatry. 2022;27:2659–73.
21. Brown LS, Foster CG, Courtney J-M, King NE, Howells DW, Sutherland BA. Pericytes and neurovascular function in the healthy and diseased brain. Front Cell Neurosci. 2019;13:282.
22. Liu L-R, Liu J-C, Bao J-S, Bai Q-Q, Wang G-Q. Interaction of microglia and astrocytes in the neurovascular unit. Front Immunol. 2020;11:1024.
23. Cabezas R, Avila M, Gonzalez J, El-Bachá RS, Báez E, García-Segura LM, et al. Astrocytic modulation of blood brain barrier: perspectives on parkinson's disease. Front Cell Neurosci. 2014;8:211.
24. Mo F, Pellerino A, Soffietti R, Rudà R. Blood-Brain barrier in brain tumors: biology and clinical relevance. Int J Mol Sci. 2021;22:12654.
25. Sarkaria JN, Hu LS, Parney IF, Pafundi DH, Brinkmann DH, Laack NN, et al. Is the blood–brain barrier really disrupted in all glioblastomas? A critical assessment of existing clinical data. Neurooncology. 2018;20:184–91.
26. Xie Y, He L, Lugano R, Zhang Y, Cao H, He Q, et al. Key molecular alterations in endothelial cells in human glioblastoma uncovered through single-cell RNA sequencing. JCI Insight. 2021;6:e150861.
27. Huang M, Zhang D, Wu JY, Xing K, Yeo E, Li C, Zhang L, Holland E, Yao L, Qin L, Binder ZA, O'Rourke DM, Brem S, Koumenis C, Gong Y, Fan Y. Wnt-mediated endothelial transformation into mesenchymal stem cell-like cells induces chemoresistance in glioblastoma. Sci Transl Med. 2020 Feb 26;12(532):eaay7522. https://doi.org/10.1126/scitranslmed.aay7522. PMID: 32102932; PMCID: PMC7261487.
28. Zeng Q, Li W, Lu D, Wu Z, Duan H, Luo Y, et al. CD146, an epithelial-mesenchymal transition inducer, is associated with triple-negative breast cancer. Proc Natl Acad Sci USA. 2011;109:1127.
29. Robey RW, Pluchino KM, Hall MD, Fojo AT, Bates SE, Gottesman MM. Revisiting the role of ABC transporters in multidrug-resistant cancer. Nat Rev Cancer. 2018;18:452–64.
30. Majchrzak-Celińska A, Sidhu A, Miechowicz I, Nowak W, Barciszewska A-M. ABCB1 is frequently methylated in Higher-Grade gliomas and May serve as a diagnostic biomarker of more aggressive tumors. J Clin Med. 2022;11:5655.
31. Cordon-Cardo C, O'Brien JP, Boccia J, Casals D, Bertino JR, Melamed MR. Expression of the multidrug resistance gene product (P-glycoprotein) in human normal and tumor tissues. J Histochem Cytochem. 1990;38:1277–87.
32. Jiang T, Zhuang J, Duan H, Luo Y, Zeng Q, Fan K, et al. CD146 is a coreceptor for VEGFR-2 in tumor angiogenesis. Blood. 2012;120:2330–9.
33. Tu T, Zhang C, Yan H, Luo Y, Kong R, Wen P, et al. CD146 acts as a novel receptor for netrin-1 in promoting angiogenesis and vascular development. Cell Res. 2015;25:275–87.
34. Yan B, Lu Q, Gao T, Xiao K, Zong Q, Lv H, et al. CD146 regulates the stemness and chemoresistance of hepatocellular carcinoma via JAG2-NOTCH signaling. Cell Death Dis. 2025;16:1–12.
35. Errede M, Mangieri D, Longo G, Girolamo F, de Trizio I, Vimercati A, et al. Tunneling nanotubes evoke pericyte/endothelial communication during normal and tumoral angiogenesis. Fluids Barriers CNS. 2018;15:28.
36. Sacchetti B, Funari A, Michienzi S, Di Cesare S, Piersanti S, Saggio I, et al. Self-renewing osteoprogenitors in bone marrow sinusoids can organize a hematopoietic microenvironment. Cell. 2007;131:324–36.
37. Covas DT, Panepucci RA, Fontes AM, Silva WA, Orellana MD, Freitas MCC, et al. Multipotent mesenchymal stromal cells obtained from diverse human tissues share functional properties and gene-expression profile with CD146 + perivascular cells and fibroblasts. Exp Hematol. 2008;36:642–54.
38. Abdoli Shadbad M, Nejadi Orang F, Baradaran B. CD133 significance in glioblastoma development: in Silico and in vitro study. Eur J Med Res. 2024;29:154.
39. Brescia P, Ortensi B, Fornasari L, Levi D, Broggi G, Pelicci G. CD133 is essential for glioblastoma stem cell maintenance. Stem Cells. 2013;31:857–69.
40. Ahmed SI, Javed G, Laghari AA, Bareeqa SB, Farrukh S, Zahid S, Samar SS, Aziz K. CD133 Expression in Glioblastoma Multiforme: A Literature Review. Cureus. 2018 Oct 11;10(10):e3439. https://doi.org/10.7759/cureus.3439. PMID: 30555755; PMCID: PMC6290980.
41. Liang Y, Voshart D, Paridaen JTML, Oosterhof N, Liang D, Thiruvalluvan A, et al. CD146 increases stemness and aggressiveness in glioblastoma and activates YAP signaling. Cell Mol Life Sci. 2022;79:398.
42. Girolamo F, Errede M, Bizzoca A, Virgintino D, Ribatti D. Central nervous system pericytes contribute to health and disease. Cells. 2022;11:1707.
43. Girolamo F, de Trizio I, Errede M, Longo G, d'Amati A, Virgintino D. Neural crest cell-derived pericytes act as pro-angiogenic cells in human neocortex development and gliomas. Fluids Barriers CNS. 2021;18:14.
44. Yawata T, Higashi Y, Kawanishi Y, Nakajo T, Fukui N, Fukuda H, et al. CD146 is highly expressed in glioma stem cells and acts as a cell cycle regulator. J Neurooncol. 2019;144:21–32.
45. Joshkon A, Tabouret E, Traboulsi W, Bachelier R, Simoncini S, Roffino S, et al. Soluble CD146, a biomarker and a target for preventing resistance to anti-angiogenic therapy in glioblastoma. Acta Neuropathol Commun. 2022;10:151.

Publisher's note

Springer Nature remains neutral with regard to jurisdictional claims in published maps and institutional affiliations.